Predicted Permeability of the Cornea to Topical Drugs

Aurélie Edwards[1,3] and Mark R. Prausnitz[2]

Purpose. To develop a theoretical model to predict the passive, steady-state permeability of cornea and its component layers (epithelium, stroma, and endothelium) as a function of drug size and distribution coefficient (Φ). The parameters of the model should represent physical properties that can be independently estimated and have physically interpretable meaning.

Methods. A model was developed to predict corneal permeability using 1) a newly developed composite porous-medium approach to model transport through the transcellular and paracellular pathways across the epithelium and endothelium and 2) previous work on modeling corneal stroma using a fiber-matrix approach.

Results. The model, which predicts corneal permeability for molecules having a broad range of size and lipophilicity, was validated by comparison with over 150 different experimental data points and showed agreement with a mean absolute fractional error of 2.43, which is within the confidence interval of the data. In addition to overall corneal permeability, the model permitted independent analysis of transcellular and paracellular pathways in epithelium, stroma and endothelium. This yielded strategies to enhance corneal permeability by targeting epithelial paracellular pathways for hydrophilic compounds ($\Phi < 0.1 - 1$), epithelial transcellular pathways for intermediate compounds, and stromal pathways for hydrophobic compounds ($\Phi > 10 - 100$). The effects of changing corneal physical properties (e.g., to mimic disease states or animals models) were also examined.

Conclusions. A model based on physicochemical properties of the cornea and drug molecules can be broadly applied to predict corneal permeability and suggest strategies to enhance that permeability.

KEY WORDS: ophthalmic drug delivery; theoretical model; eye; ophthalmology; ocular transport prediction.

INTRODUCTION

Topical drug delivery to the eye is the most common treatment of ophthalmic diseases, and the cornea provides the dominant barrier to drug transport (1). For this reason, a large body of experimental work has characterized corneal permeability (2), and some models have been developed as a result to describe transcorneal transport (3–7). However, most existing models rely on parameters that are fitted to a small number of experimental measurements and are not applicable to larger data sets, and many models do not account for all existing transport processes and routes. A model that can predict the corneal permeability of any drug based on its

---
[1] Department of Chemical and Biological Engineering, Tufts University, 4 Colby Street, Medford, Massachusetts 02155.
[2] Schools of Chemical and Biomedical Engineering, Georgia Institute of Technology, Atlanta, Georgia 30332–0100.
[3] To whom correspondence should be addressed. (e-mail: aurelie.edwards@tufts.edu)

physical properties and those of the cornea would be more broadly useful.

If all the variables of a predictive model correspond to physical properties that are independently measured (such as molecular radius, width of intercellular spaces, etc.), the model then should not only describe the data used in its development but also predict corneal permeability to classes of compounds not considered during model development. With such a tool, the ability to deliver newly synthesized or even computer-generated drugs can be assessed without stepping into the laboratory. In addition, transport processes can be understood in physical terms (e.g., epithelial tight junctions are the rate-limiting barrier for a given drug), which helps develop appropriate ways to enhance or target delivery and facilitates predicting or analyzing delivery problems. Finally, because model variables have physical meaning, they can be easily changed to reflect the properties of diseased or injured cornea and to account for differences between humans and animals.

Given the potential power of an approach based on physics rather than statistics, we developed a model that builds off of previous work describing the permeability of corneal stroma (and sclera) by modeling it as a fiber matrix (8) and combines it with a new analysis presented for the corneal epithelium and endothelium. Both transcellular and paracellular transport pathways were considered and, whenever possible, parameters were derived from independent experimental observations.

MODEL DEVELOPMENT

Following the general approach taken by a number of previous studies (4,6,9), the steady-state permeability of cornea can be determined by considering the individual permeabilities of the three primary tissues that make up cornea: endothelium, stroma, and epithelium (10). Because Bowmann's membrane and Descemet's membranes are so thin and permeable, they do not contribute significantly to overall corneal permeability and are therefore not considered in this analysis. We have developed previously a model that predicts the permeability of stroma and that of the paracellular pathway across endothelium (8). In this section, we summarize these findings and develop new expressions for transport across the epithelium and the transcellular pathway across endothelium.

Endothelium

The corneal endothelium is a monolayer of hexagonal cells, each about 20 μm wide and 5 μm thick, found at the internal base of the cornea (10). Two pathways are available for solutes diffusing across the endothelium (Fig. 1): a paracellular route (i.e., between cells), which is a water-filled pathway impeded by gap and tight junctions and is favored by hydrophilic molecules and ions; and a transcellular route (i.e., within or across cell membranes), which involves partitioning into and diffusing within cell membranes and is the pathway of choice for hydrophobic molecules. The fraction of a given solute that goes through each route is determined primarily by its membrane-to-water distribution coefficient (Φ). The larger Φ (i.e., for hydrophobic molecules), the greater the
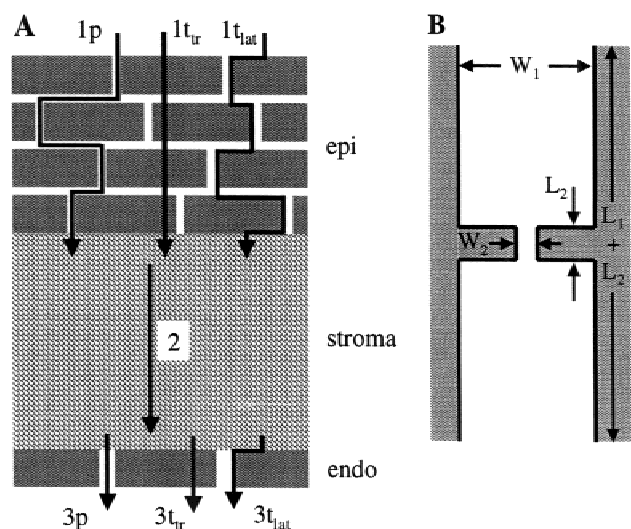
Fig. 1. An idealized representation of the cornea showing transport pathways across the epithelium, stroma, and endothelium (drawing not to scale). (A) In the epithelium, paracellular pathways follow the hydrophilic spaces between epithelial cells ($1p$), and transcellular pathways are either solely within the hydrophobic cell membranes ($1t_{lat}$) or alternate crossing of cell membranes and cell cytosol ($1t_{tr}$). The largely cell-free stroma offers only hydrophilic pathways among and between collagen fibers and proteoglycan matrix (2). The endothelium contains both hydrophilic paracellular ($3p$) and hydrophobic transcellular ($3t_{lat}$ and $3t_{tr}$) routes. (B) The paracellular spaces in epithelium and endothelium are modeled as slits with constrictions that represent tight and gap junctions.

relative amount of solute that diffuses through the cells. Because the two pathways are in parallel, the overall permeability of the cell layer (k_{layer}) is the sum of the permeabilities of each pathway:

$$k_{layer} = k_t + k_p \tag{1}$$

where k_t and k_p are the permeabilities of transcellular and paracellular routes, respectively. How to calculate the permeability of each of these pathways is described below.

Transcellular Pathway

The transcellular pathway across endothelium involves two possible routes. The first route consists of 1) partitioning from the water-rich stroma into the lipid-rich plasma membranes of endothelial cells; 2) diffusing within the cell membranes across the endothelium; and 3) partitioning out of the membranes and into the aqueous humor bathing the internal surface of the cornea. This pathway, referred to as the lateral route of the transcellular pathway (pathway $3t_{lat}$ in Fig. 1A), does not include transport within the cytosol of endothelial cells. The second route involves the following: 1) partitioning into, diffusing transversely across, and partitioning out of the anterior cell membrane; 2) diffusing through the cytosol; and 3) partitioning into, diffusing across, and partitioning out of the posterior cell membrane. This second pathway is referred to as the transverse route (pathway $3t_{tr}$ in Fig. 1A).

For simplicity, we assume those two routes can be treated separately. In reality, they are not independent: a molecule may follow a path involving a combination of lateral transport along the membrane and diffusion in the cytosol. Given this

the overall permeability of the transcellular route can be expressed as:

$$k_t = k_{lat} + k_{tr} \tag{2}$$

where k_{lat} and k_{tr} are the permeabilities of the lateral and transverse routes, respectively.

Lateral Diffusion. The permeability k_{lat} of the lateral transcellular pathway to a given solute is given by:

$$k_{lat} = \frac{\Phi D_{lat}}{L_{lat}} \tag{3}$$

where D_{lat} is the lateral diffusivity of the solute in the cell membranes and L_{lat} is the mean diffusion pathway length.

Our estimate of the lateral diffusivity of a small solute (~5 Å in radius) in the cell membranes of the cornea is 2×10^{-8} cm^2/s, based upon a compilation of experimental measurements reported by Johnson *et al.* (11), which were conducted using model cholesterol-containing lipid bilayers. This value is consistent with membrane diffusion studies in epithelial tissues (12). The mean diffusion pathway length, L_{lat}, was calculated as described below (Eq. 12). The average length of the paracellular opening between adjacent endothelial cells is $L = 12.2$ μm (13), and the average radius of an endothelial cell is 10 μm, yielding $L_{lat} = 12.2 + 10/3 = 15.5$ μm.

An empirical relationship between the membrane-to-water distribution coefficient and that between octanol and water (K_{ow}) is given by Johnson (Mark Johnson, personal communication):

$$\Phi = K_{ow}^{0.87} \tag{4}$$

The octanol-to-water distribution coefficient was determined using experimental values for the octanol-to-water partition coefficient and calculated values of the degree of solute ionization (assuming ionized molecules do not partition into octanol), as described and tabulated in Prausnitz and Noonan (2).

Transverse Diffusion. The permeability of the transverse route, k_{tr}, was calculated by considering three steps in series: transport across the anterior endothelial cell membrane, diffusion through cell cytoplasm, and transport across the posterior cell membrane.

$$\frac{1}{k_{tr}} = \frac{1}{k_{mem}} + \frac{1}{k_{cyt}} + \frac{1}{k_{mem}} = \frac{2}{k_{mem}} + \frac{1}{k_{cyt}} \tag{5}$$

where k_{mem} is cell membrane permeability and k_{cyt} is trans-cytosol permeability.

Endothelial cell membrane permeability was difficult to calculate because very few independent data are available. Most membrane permeability studies have used artificial lipid bilayers, which are more permeable than cell membranes. Lacking data on endothelial cell membrane permeability, we chose red blood cell (RBC) membranes as a model, which is the only cell membrane for which we could find useful data on transmembrane transport by passive mechanisms (i.e., diffusion).

Reliable measurements of RBC basal permeability have been compiled by Lieb and Stein (14). The octanol-to-water partition coefficient of the solutes considered in that study varies over a broad range between 1.2×10^{-3} and 1.1×10^{2}, but their molecular volume does not exceed 73 cm^3/mol (i.e., ~3 Å radius), meaning that data extrapolation was needed to include molecules typically delivered to the eye (i.e., radius of 3.5 to 5.5 Å). Recognizing this limitation, we used the model of Lieb and Stein for non-Stokesian diffusion (14), whereby the permeability of a cell membrane can be written as

$$k_{mem} = k_{mem}^0 \, 10^{-m_v V} \qquad (6)$$

where k_{mem}^0 is the membrane permeability for a theoretical molecule of infinitely small size and the term $10^{-m_v V}$ accounts for the effects of molecular size; m_v is a measure of the size selectivity for diffusion within the membrane, which is 0.0516 mol/cm^3 for human RBCs (14), and V is the van der Waals molecular volume determined from molecular structure (2). The term K_{mem}^0 has been empirically shown to depend on partition coefficient according to the following relationship.

$$\log(k_{mem}^0) = A \log(K_{ow}) + B \qquad (7)$$

where k_{mem}^0 has units of cm/s. Using octanol as a model for partitioning and assuming that the values of the distribution and partition coefficients are similar for the solutes being considered, the best-fit values of A and B were found to be 1.323 and –0.834, respectively, by linear regression of the RBC permeability data presented by Lieb and Stein (14).

Once the solute has crossed the cell membrane, it will diffuse within the cell cytoplasm. Cytosol-to-water diffusivity ratios have been found to be on the order of 1/4 (15), and we assumed that the average distance traveled within the cytosol from one side of the cell to the other is about $l_{cyt} = 5$ μm. The transcytosol permeability can thus be estimated as follows:

$$k_{cyt} = \frac{D_\infty}{4 l_{cyt}} \qquad (8)$$

where D_∞ is the solute diffusivity in dilute bulk solution. Implicit in the equation given above is the assumption that solubility within the cytoplasm is equal to that within water.

Equation 6 yields transverse permeability values that are very low and almost always negligible compared to lateral permeability values. Because the data of Lieb and Stein (14) were obtained for molecular radii smaller than about 3 Å, it is possible that the expression accounting for the size dependence of k_{mem} does not apply to the larger solutes examined in this study. If Equation 6 overpredicts permeability (i.e., the actual transverse permeability is lower), overall model predictions would remain unchanged, because the transverse route would remain negligible. In contrast, underprediction could be problematic because transverse permeabilities could become significant and thereby increase corneal permeability predictions.

To assess the likelihood of over- or underprediction for larger molecules, we found literature values for transverse permeability across synthetic lipid bilayers for tryptophan ($K_{ow} = 9.1 \times 10^{-2}$) and citric acid ($K_{ow} = 1.9 \times 10^{-2}$), both of which have a radius of about 3.5 Å (16,17). These permeabilities have been measured as 4.1×10^{-10} and 3.1×10^{-11} cm/s, respectively, whereas Equation 6 predicts values of 1.6×10^{-8} and 2.1×10^{-9} cm/s, respectively. Although this large over-

prediction reduces our confidence in extrapolated predictions using Equation 6, it supports our overall conclusion that the transverse route is almost always negligible, because these measured permeabilities are even smaller than predicted.

Paracellular Pathway

Solutes that do not partition extensively into endothelial cell membranes and thus cannot access the transcellular pathway follow the paracellular route between the cells. As described by Fischbarg (13), the intercellular space between two endothelial cells can be idealized as a slit channel consisting of a wide section and a narrow one, the latter corresponding to the gap junction (Fig. 1B). The half-width of the wide part (W_1) and that of the narrow part (W_2) have been measured as 15 nm and 1.5 nm, respectively. The length of the wide part (L_1) has been determined to be 12 μm and that of the gap junction (L_2) is 0.24 μm (13).

Based on the theoretical results of Panwar and Anderson (18), the permeability k_i of a parallel-wall channel of half-width W_i and length L_i is given by:

$$k_i = \frac{f_i D_\infty}{L_i} \left[1 + \frac{9}{16} \left(\frac{r_s}{W_i} \right) \ln \left(\frac{r_S}{W_i} \right) - 1.19358 \left(\frac{r_s}{W_i} \right) + 0.159317 \left(\frac{r_s}{W_i} \right)^3 \right] \qquad (9)$$

where f_i is the fractional area of intercellular openings on the surface (i.e., porosity), and r_s is the solute radius. The total cell perimeter length per unit area is $l_c = 1200$ cm/cm^2 of endothelial surface (13), and f_i is estimated as $W_i \cdot l_c$. The term within brackets in Equation 9 represents the channel-to-free solution diffusivity ratio (including the effects of partitioning). D_∞ is determined using the Wilke-Chang equation (19) (for the molecules examined in this study, D_∞ is between 0.5×10^{-5} and 2×10^{-5} cm^2/s). Electrostatic effects are neglected in this approach, as suggested by previous studies (20). Also, note that because of tortuosity, the total length of the intercellular channel, $L_1 + L_2 = 12.2$ μm, is significantly greater than the cell thickness, which is equal to 5 μm.

The overall permeability of the paracellular pathway, consisting of the wide and narrow slit channels in series, is then given by:

$$k_p = \frac{1}{1/k_1 + 1/k_2} \qquad (10)$$

Stroma

The stroma is a fibrous tissue that forms the bulk of the cornea and is made up primarily of large collagen fibers embedded in a proteoglycan matrix. We previously developed a model for the permeability of the stroma to small solutes and macromolecules (8). The analysis was performed on three length scales; for each, we assumed a given arrangement of fibers of defined geometry and orientation, around and through which solutes diffuse. Corresponding calculations were based on a fiber matrix approach. At the macroscale, stromal collagen lamellae are arranged in parallel sheets. At the mesoscale, the lamellae contain collagen fibrils forming hexagonal arrays of parallel cylinders. At the microscale, ground substance that surrounds the fibrils and lamellae was modeled as a randomly oriented collection of fibers, repre-

senting the proteoglycans. The corresponding equations are detailed in Edwards and Prausnitz (8) and are briefly summarized in the Appendix. It should be noted that in the previous study (8), a stromal hydration of 86% was used because we considered transport across isolated stroma, which has an increased water content. For this study, stromal hydration was taken as 78%, which is the physiologic value for intact cornea (8,10).

Epithelium

The epithelium is a multi-layer of cells found at the external surface of the cornea. The basal layer, separated from the stroma by a thin basement membrane, consists of a single sheet of columnar cells, about 20 μm high and 10 μm wide (10). Two or three layers of wing cells cover the basal cells, from which they are derived. As wing cells migrate towards the corneal surface, they flatten and give rise to two or three sheets of squamous cells that are about 4 μm thick and 20–45 μm wide. The total thickness of corneal epithelium is approximately 50–60 μm in humans (10). Similar to endothelium, the epithelium has two parallel pathways, a transcellular and a paracellular one (Fig. 1), meaning that Eq. 1 can be used.

Transcellular Pathway

The permeability of the transcellular pathway in the epithelium was calculated using Eq. 2; the values for k_{lat} and k_{tr} were determined as follows.

Lateral Diffusion. The permeability of the lateral route in the epithelium was calculated using Eq. 3, assuming that the only significant difference between lateral diffusion across corneal epithelium and endothelium is the pathway length, L_{lat}. That is, Φ and D_{lat} have the same values as in endothelium. We assumed that epithelial cells are packed very tightly so that there is almost no discontinuity as a solute diffuses from one cell to the other, i.e., membrane-to-membrane partitioning is not a rate-limiting step.

The mean diffusion pathway length, L_{lat}, was calculated assuming the cells are shaped like cylinders. Once a molecule partitions into a cell membrane somewhere on its upper surface, it must first diffuse across to the edge of the upper surface and then down along the side of the cell. The average distance $\langle r_i \rangle$ a molecule must diffuse across the upper circular surface of a cell i is equal to:

$$\langle r_i \rangle = R_i - \frac{1}{\pi R_i^2} \int_{r=0}^{R_i} \int_{\theta=0}^{2\pi} r^2 dr d\theta = \frac{R_i}{3} \qquad (11)$$

where R_i is the cell radius.

Assuming that the cells do not form columns but are randomly aligned, the mean pathway length is then given by:

$$L_{lat} = \sum_i \left(L_i + \frac{R_i}{3} \right) = L + \frac{1}{3}\sum_i R_i \qquad (12)$$

where L_i is the distance that a molecule must diffuse down along the side of a cell and L is the total diffusion length along the side of the cells, which is greater than the thickness of the epithelium because of tortuosity. In the 5-μm-thick endothelium, L has been measured as approximately 12 μm, i.e., a tortuosity of 2.4 (13). In the absence of data for the epithelium, we assumed that the tortuosity factor was the same in both barriers, and L was taken as 120 μm for the 50-μm-thick

epithelium. In addition, we assumed an idealized epithelial geometry having three layers of squamous cells with a mean surface radius of 20 μm, three layers of wing cells of mean radius 10 μm, and one layer of columnar cells, 5 μm in radius (10). This yields L_{lat} = 120 + 95/3 = 151.7 μm.

Transverse Diffusion. To determine the permeability of the transverse route across epithelium, the permeability of a single cell membrane and that of the cytosol in a single cell were taken to be the same as in endothelium. Because epithelial cell layers can be represented as resistances in series, l_{cyt} was set equal to epithelium thickness, 50 μm, and Eq. 8 was used to calculate cytosol permeability. The permeability of a single cell membrane was determined using Eq. 6, and Eq. 5 was used to calculate permeability of the transverse route with the term $1/k_{mem}$ multiplied by 14, rather than 2, based on our above idealization of seven cell layers in the epithelium.

Paracellular Pathway

Freeze-fracture observations of the epithelium show that tight junctions are localized almost exclusively in the superficial layer, whereas larger gap junctions are found in deeper layers (21). In the absence of specific experimental data regarding the dimensions of the different epithelial junctions, we chose to replace those multiple junctions by one narrow junction, such that the latter would account for the size selectivity imparted by all tight and gap junctions combined. We therefore modeled each intercellular opening as a parallel-wall slit with a narrow section, corresponding to the equivalent junction, followed by a wider one (Fig. 1B). The dimensions of the epithelial narrow junction were chosen so that its effects are equivalent to the combined effects of all epithelial junctions in series, as described below.

Lacking independent data, the large half-width (W_1) was taken to be 15 nm throughout the epithelium, which was based on measurements in endothelium. We estimated the narrow half-width (W_2) based upon the data of Hämäläinen *et al.* (22). In their study, the authors measured the permeability of cornea to small hydrophilic solutes, which diffuse predominantly through the paracellular pathway and for which the epithelium should be by far the tightest barrier. We therefore fitted Eq. 10 to their data; the value of W_2 that yielded the best agreement with experimental observations was 0.8 nm. We further assumed that the length of the equivalent narrow junction in the epithelium was L_2 = 0.24 μm, that is, equal to that of endothelial gap junctions. The combined length of the wide channel parts (L_1) was assumed to be equal to the overall distance covered by molecules diffusing alongside the edge of cells minus the length of the tight junction, i.e., $L_{lat} - L_2$ = 151.4 μm.

Given a cell density of $1/(\pi R_i^2)$, the total cell perimeter length per unit area of epithelium, l_c, was calculated as $2/R_i$ (i.e., 1000 cm/cm^2 based on a 20 μm radius for squamous cells; Ref. 15), and f_i was calculated as $W_i \cdot l_c$. With those parameters, the permeability of the paracellular pathway in epithelium was determined using Eqs. 9 and 10.

Whole Cornea

In summary, solute permeability of epithelium and endothelium is each described by the sum of the transcellular

(Eq. 2) and paracellular (Eq. 10) contributions, where different geometric constants (e.g., L_i, L_{lat}, W_i) are used in each tissue, as summarized in Table I. The permeability of stroma is calculated using a fiber-matrix model developed previously (8) and briefly recapitulated in the Appendix. Finally, the overall permeability of the cornea (k_{cornea}) is determined by the series combination of the resistance to transport of the three tissues:

$$\frac{1}{k_{cornea}} = \frac{1}{k_{epi}} + \frac{1}{k_{stroma}} + \frac{1}{k_{endo}} \tag{13}$$

where the subscripts "epi" and "endo" refer to the epithelium and endothelium, respectively.

Calculations for Model Validation and Comparison with Other Theoretical Models

Comparisons between model predictions and experimental data are needed to validate the above model, which we performed using a compilation of experimentally determined permeabilities, as well as distribution coefficients, molecular radii, and other data collected by Prausnitz and Noonan (2). Whole cornea and isolated stroma permeabilities were determined directly through experimentation. However, few direct experimental measurements of corneal endothelial or epithelial solute permeability were made. Instead, literature reports present permeability values for combined layers, such as stroma-plus-endothelium, i.e., de-epithelialized cornea. Indirect experimental values of the permeability of endothelium and epithelium were therefore obtained by considering resistances in series. For example, endothelial permeabilities were determined by subtracting the resistance (i.e., the inverse of the permeability) of stroma from that of stroma-plus-endothelium:

$$\frac{1}{k_{endo}} = \frac{1}{k_{stroma+endo}} - \frac{1}{k_{stroma}} \tag{14}$$

Epithelial permeabilities were calculated in a similar manner, based on reported values for stroma and stroma-plus-epithelium, or for full cornea and de-epithelialized cornea.

These calculations require that the measured values that are combined to yield endothelial or epithelial permeabilities correspond to identical experimental conditions, i.e., same species, temperature, and hydration. We therefore only subtracted resistances when they were reported in the same study. Even in this case, it is, for example, likely that the hydration of stroma was higher when the cell layers were removed, but we did not account for this effect in the absence of specific hydration data. Results for endothelium and epithelium are given in Tables II and III, respectively. In some studies, the measured permeability of several layers com-

bined was higher than that of one layer; such inconsistent data were not included in this analysis.

Uncertainties in these permeability values can be very large, as illustrated by the following example. The reported permeability of stroma to corynanthine is $3.2 \pm 0.6 \times 10^{-5}$ cm/s and that of stroma-plus-endothelium is $3.1 \pm 0.2 \times 10^{-5}$ cm/s (23), yielding a calculated endothelial permeability of $9.9 \pm 78 \times 10^{-4}$ cm/s. Even though experimental standard deviations were small, uncertainty in k_{endo} is much larger than the permeability itself because the two measured values are very close. This constrains our ability to validate model predictions given the large error bars on much of the test data calculated using Eq. 14.

To compare the predictive ability of our model to that of others, we calculated the following sum of squared errors, which is related to a log-scale chi squared (24):

$$SSE = \sum_{i=1}^{n} \left[\frac{\ln(k_{cornea}^{calc})}{\ln(k_{cornea}^{meas})} - 1 \right]^2 \tag{15}$$

where n is the number of solutes considered (e.g., 117 for the cornea) and k_{cornea}^{calc} and k_{cornea}^{meas} are the calculated and measured permeabilities of cornea to solute i, respectively. As an additional characterization, we determined the mean absolute fractional error (MAFE) associated with differences between predicted and measured values, defined as the average absolute value of the residual divided by the actual (i.e., experimental) value (24).

$$MAFE = \frac{1}{n} \sum_{i=1}^{n} \frac{|k_{cornea}^{calc} - k_{cornea}^{meas}|}{k_{cornea}^{meas}} \tag{16}$$

RESULTS AND DISCUSSION

Permeability Predictions

To predict the passive, steady-state permeability of cornea to a broad range of compounds, we developed a theoretical model based on the physicochemical properties of the cornea and diffusing solutes, which were estimated, whenever possible, from independent literature data. Two types of pathways were considered (Fig. 1). Paracellular pathways are water-filled routes between cells in epithelium and endothelium and between the fibers of the largely aqueous stroma. Permeability of these routes is mainly a function of the size and geometry of the pathways and solutes. Transcellular pathways consist of lipid-filled routes within cell membranes. Although the permeability of those pathways also depends upon size and geometry, another important factor is the ability of a solute to partition into cell membranes, as determined by the solute's membrane-to-water distribution coefficient.

Table I. Parameters for Epithelial and Endothelial Permeability Calculations

	Endothelium	Epithelium
Transcellular mean diffusion pathway length (L_{lat})	15.5 μm	151.7 μm
Lateral diffusivity in cell membranes (D_{lat})	2×10^{-8} cm²/s	2×10^{-8}/cm²/s
Wide channel half-width (W_1)	15 nm	15 nm
Narrow channel half-width (W_2)	1.5 nm	0.8 nm
Wide channel length (L_1)	12 μm	151.4 μm
Narrow channel length (L_2)	0.24 μm	0.24 μm

DOCKET ALARM

Explore Litigation Insights

Docket Alarm provides insights to develop a more informed litigation strategy and the peace of mind of knowing you're on top of things.

Real-Time Litigation Alerts

Keep your litigation team up-to-date with **real-time alerts** and advanced team management tools built for the enterprise, all while greatly reducing PACER spend.

Our comprehensive service means we can handle Federal, State, and Administrative courts across the country.

Advanced Docket Research

With over 230 million records, Docket Alarm's cloud-native docket research platform finds what other services can't. Coverage includes Federal, State, plus PTAB, TTAB, ITC and NLRB decisions, all in one place.

Identify arguments that have been successful in the past with full text, pinpoint searching. Link to case law cited within any court document via Fastcase.

Analytics At Your Fingertips

Learn what happened the last time a particular judge, opposing counsel or company faced cases similar to yours.

Advanced out-of-the-box PTAB and TTAB analytics are always at your fingertips.

API

Docket Alarm offers a powerful API (application programming interface) to developers that want to integrate case filings into their apps.

LAW FIRMS

Build custom dashboards for your attorneys and clients with live data direct from the court.

Automate many repetitive legal tasks like conflict checks, document management, and marketing.

FINANCIAL INSTITUTIONS

Litigation and bankruptcy checks for companies and debtors.

E-DISCOVERY AND LEGAL VENDORS

Sync your system to PACER to automate legal marketing.

fastcase
Smarter legal research.